Local control theory in trajectory-based nonadiabatic dynamics

Basile F. E. Curchod
Laboratory of Computational Chemistry and Biochemistry, Ecole Polytechnique Fédérale de Lausanne, CH-1015 Lausanne, Switzerland

Thomas J. Penfold*
Laboratory of Computational Chemistry and Biochemistry, Ecole Polytechnique Fédérale de Lausanne, CH-1015 Lausanne, Switzerland, Ecole Polytechnique Fédérale de Lausanne, Laboratoire de Spectroscopie Ultrarapide, ISIC, FSB-BSP, CH-1015 Lausanne, Switzerland, SwissFEL, Paul Scherrer Institut, CH-5232 Villigen, Switzerland

Ursula Rothlisberger and Ivano Tavernelli†
Laboratory of Computational Chemistry and Biochemistry, Ecole Polytechnique Fédérale de Lausanne, CH-1015 Lausanne, Switzerland
(Received 16 August 2011; published 12 October 2011)

In this paper, we extend the implementation of nonadiabatic molecular dynamics within the framework of time-dependent density-functional theory in an external field described in Tavernelli *et al*. [Phys. Rev. A **81**, 052508 (2010)] by calculating on-the-fly pulses to control the population transfer between electronic states using local control theory. Using Tully's fewest switches trajectory surface hopping method, we perform MD to control the photoexcitation of LiF and compare the results to quantum dynamics (QD) calculations performed within the Heidelberg multiconfiguration time-dependent Hartree package. We show that this approach is able to calculate a field that controls the population transfer between electronic states. The calculated field is in good agreement with that obtained from QD, and the differences that arise are discussed in detail.

DOI: 10.1103/PhysRevA.84.042507 PACS number(s): 31.10.+z, 31.15.ee, 71.15.Pd, 31.50.Gh

I. INTRODUCTION

Nonadiabatic molecular dynamics schemes, of which the most well known is Tully's trajectory surface hopping (TSH) [1], discretizes the wave packet into a swarm of independent classical trajectories and accounts for electronic-nuclear coupling effects by the *hops* of the trajectories between different electronic states according to a stochastic algorithm calculated as a function of the nonadiabatic couplings (NACs). Its ability to accurately describe nonadiabatic dynamics has led to it becoming a widely used approach with successful applications to a range of chemical problems [2–7]. The condition of spatial locality enforced by the discretization of the wave packet makes trajectory-based methods ideal for the implementation of on-the-fly molecular dynamics (MD), meaning that the energies and nuclear forces are only required at the current point in coordinate space (a δ function) of the trajectory. As a result, TSH has been coupled with a variety of electronic structure methods described in a recent paper [8].

Most recently TSH has been implemented on-the-fly within the linear-response time-dependent density-functional theory (LR-TDDFT) framework [9–13], following the proposed schemes for calculating the nonadiabatic coupling vectors (NACVs) within LR-TDDFT using a set of auxiliary many-electron wave functions [14–18]. Further extensions by Tavernelli *et al*. [19], Mitrić *et al*. [20], Petersen *et al*. [21], and Mitrić *et al*. [22,23] have included the effect of an external field. Outside LR-TDDFT, it is interesting to note the recent contribution of Richter *et al*., who proposed an extension of surface hopping to arbitrary couplings (external-field and spin-orbit couplings) called SHARC (surface hopping in adiabatic representation including arbitrary couplings) [24]. By considering the effect of an electric field, one is able to study the response of a system under such a perturbation; furthermore, by careful design of the frequency-time evolution of this field, one can control the dynamics of the system, driving the trajectory into the region of interest.

The control of molecular processes by shaped laser fields has been applied to a wide variety of systems since it was pioneered in the mid-1980s by the Tannor-Rice pump-dump [25] and the Brumer-Shapiro schemes [26]. Theoretically, the most standardly used approach for coherent control is optimal control theory (OCT) [27], which is analogous to the commonly used experimental learning algorithm approach [28]. This technique uses a variational principle and an iterative process of forward and backward propagations to construct a field that guides the wave function optimally toward a predefined target wave function. However, its numerical implementation is extremely computationally expensive due to the multiple forward-backward propagations.

Local control theory (LCT) offers an attractive alternative for calculating the external field because it can be calculated and can be applied on-the-fly. This approach diverges from the global optimization approach of OCT by the fact that the field is calculated to ensure an increase (or decrease) in the expectation value of one particular aspect of the system, such as a specific electronic state population, vibrational state population, or nuclear motion. The requirement for it to be a function of some expectation value offers a large flexibility within the method. This approach has been applied successfully to photoexcitation, photoinduced molecular fragmentation, and association and vibrational stabilizations [29–31]. Recently, Penfold *et al*. [32] studied the controlled excitation of simple hydrocarbons using potential energy surfaces (PESs), which

*thomas.penfold@epfl.ch
†ivano.tavernelli@epfl.ch

exhibited strong nonadiabatic effects, while Kritzer *et al.* [33] studied the effect of environmental perturbations on the excitation in Na_2. A detailed review can be found in Ref. [34].

In this paper, we present the implementation of LCT within a trajectory surface hopping *ab initio* MD scheme. All of the relevant quantities, namely, electronic energies, nuclear forces, NACVs, and transition dipole elements are calculated on-the-fly within LR-TDDFT [19] as implemented in the software package CPMD [35]. The results are compared with quantum dynamics (QD) calculations performed within the Heidelberg multiconfiguration time-dependent Hartree (MCTDH) package [36], using the PESs extracted from DFT–LR-TDDFT calculations with CPMD. Comparison between TSH and QD has been performed previously and can be found within Refs. [37,38] and [20] (the latter also includes an external field). However, here, we pay particular attention to the comparison between the dynamics induced by the pulses calculated using LCT within the two approaches and rationalize the approximations.

II. THEORY

In this section, we outline the formulation of nonadiabatic MD and the interaction with an external perturbation. This has been presented in detail in Ref. [19], and therefore, we present only a summary for reference. The description of the interaction with the light field is then developed to incorporate LCT.

A. Nonadiabatic dynamics

We start from the nonrelativistic time-dependent Schrödinger equation for a molecular system composed of nuclei and electrons,

$$\hat{H}\Psi(\boldsymbol{r},\boldsymbol{R},t) = i\hbar\frac{\partial}{\partial t}\Psi(\boldsymbol{r},\boldsymbol{R},t), \tag{2.1}$$

where $\hat{H} = \hat{T}_N + \hat{\mathcal{H}}_{el}$ is the molecular time-independent Hamiltonian, $\Psi(\boldsymbol{r},\boldsymbol{R},t)$ is the total wave function of the system under investigation, $\boldsymbol{r}$ is the collective position vector of all electrons $\{\boldsymbol{r}_i\}$, and $\boldsymbol{R}$ is the collective position vector of the nuclei $\{\boldsymbol{R}_\gamma\}$. In order to derive our working equations, we use the Born-Huang [39] ansatz for the total wave function,

$$\Psi(\boldsymbol{r},\boldsymbol{R},t) = \sum_I^\infty \Phi_I(\boldsymbol{r};\boldsymbol{R})\Omega_I(\boldsymbol{R},t), \tag{2.2}$$

where $\{\Phi_I(\boldsymbol{r};\boldsymbol{R})\}$ describes a complete set of electronic basis functions that are solutions of the time-independent electronic Schrödinger equation $\hat{\mathcal{H}}_{el}(\boldsymbol{r};\boldsymbol{R})\Phi_I(\boldsymbol{r};\boldsymbol{R}) = E_I^{el}(\boldsymbol{R})\Phi_J(\boldsymbol{r};\boldsymbol{R})$ and depend parametrically on the nuclear coordinates $\boldsymbol{R}$. $E_I^{el}(\boldsymbol{R})$ is called the Ith PES, which is a function of the nuclear coordinates $\boldsymbol{R}$.

Inserting ansatz (2.2) into the time-dependent Schrödinger equation and multiplying from the left by $\Phi_J^*(\boldsymbol{r};\boldsymbol{R})$, we get, after integration over $\boldsymbol{r}$, an equation for the temporal evolution of the nuclear wave function $\chi_J(\boldsymbol{R},t)$,

$$\begin{aligned} i\hbar\frac{\partial\chi_J(\boldsymbol{R},t)}{\partial t} = &-\sum_\gamma \frac{\hbar^2}{2M_\gamma}\nabla_\gamma^2\chi_J(\boldsymbol{R},t) + \sum_I H_{JI}(\boldsymbol{R})\chi_I(\boldsymbol{R},t) \\ &+\sum_{\gamma I}\frac{\hbar^2}{2M_\gamma}D_{JI,\gamma}(\boldsymbol{R})\chi_I(\boldsymbol{R},t) \\ &-\sum_{\gamma,I\neq J}\frac{\hbar^2}{M_\gamma}\boldsymbol{d}_{JI,\gamma}(\boldsymbol{R})\nabla_\gamma\chi_I(\boldsymbol{R},t), \end{aligned} \tag{2.3}$$

where

$$H_{JI}(\boldsymbol{R}) = \int \Phi_J^*(\boldsymbol{r};\boldsymbol{R})\hat{\mathcal{H}}_{el}\Phi_I(\boldsymbol{r};\boldsymbol{R})d\boldsymbol{r}, \tag{2.4}$$

$\boldsymbol{d}_{JI,\gamma}(\boldsymbol{R})$ are the first-order nonadiabatic coupling vectors, defined as

$$\boldsymbol{d}_{JI,\gamma}(\boldsymbol{R}) = \int \Phi_J^*(\boldsymbol{r};\boldsymbol{R})[\nabla_\gamma\Phi_I(\boldsymbol{r};\boldsymbol{R})]d\boldsymbol{r}, \tag{2.5}$$

and $D_{JI,\gamma}(\boldsymbol{R})$ are the second-order nonadiabatic coupling elements given by

$$D_{JI,\gamma}(\boldsymbol{R}) = \int \Phi_J^*(\boldsymbol{r};\boldsymbol{R})\left[\nabla_\gamma^2\Phi_I(\boldsymbol{r};\boldsymbol{R})\right]d\boldsymbol{r}. \tag{2.6}$$

In order to reduce the computational expense associated with the propagation of a nuclear wave packet, Tully proposed an approximate solution of this coupled set of equations based on the so-called *independent trajectory approximation* (ITA), which is known as TSH. First, the nuclear wave packet $\chi_J(\boldsymbol{R},t)$ in the expansion (2.3) is replaced by the complex-valued time-dependent amplitude $C_J^\alpha(t)$, which apportions trajectories (labeled by α) among electronic states according to the correct quantum probability so that

$$|\Omega_J(\boldsymbol{R},t)|^2 \sim \frac{1}{M}\sum_{\{\alpha\}}\int_{t=0}^\infty dt'\left|C_J^\alpha(t')\right|^2\delta[\boldsymbol{R}-\boldsymbol{R}^\alpha(t')]\delta(t-t'), \tag{2.7}$$

once a sufficient number of trajectories has been sampled. The relation holds due to the ITA assumption, while the $\boldsymbol{R}$ dependence of the $C_J^\alpha(t)$ coefficients is determined by the initial conditions only $\boldsymbol{R}(t=0)$ and Tully's equations of motion for the nuclei. The time-dependent differential equation for the amplitudes $C_J^\alpha(t)$ is obtained by replacing

$$\Psi^\alpha(\boldsymbol{r},\boldsymbol{R},t) = \sum_J^\infty C_J^\alpha(t)\Phi_J(\boldsymbol{r};\boldsymbol{R}) \tag{2.8}$$

in the time-dependent Schrödinger equation for the electrons and reads (in the Schrödinger representation)

$$i\hbar\dot{C}_J^\alpha(t) = \sum_I C_I^\alpha(t)\left(H_{JI} - i\hbar\dot{\boldsymbol{R}}^\alpha\cdot\boldsymbol{d}_{JI}^\alpha\right), \tag{2.9}$$

where the label α indicates that the corresponding quantities are evaluated for the trajectory α of the ensemble of trajectories. The classical trajectories evolve adiabatically according to Born-Oppenheimer dynamics until a *hop* between two potential energy surfaces ($H_{II} = E_I^{el}$ and $H_{JJ} = E_J^{el}$) occurs with a probability given by a Monte Carlo-type procedure. In

the fewest switches algorithm [1], the transition probability from state I to state J in the time interval $[t,t+dt]$ is

$$g^{\alpha}_{IJ}(t,t+dt) = 2\int_{t}^{t+dt} d\tau \frac{\mathrm{Im}\left[C^{\alpha}_{J}(\tau)C^{\alpha *}_{I}H_{JI}(\tau)\right] - \mathrm{Re}\left[C^{\alpha}_{J}(\tau)C^{\alpha *}_{I}(\tau)\Xi^{\alpha}_{JI}(\tau)\right]}{C^{\alpha}_{I}(\tau)C^{\alpha *}_{I}(\tau)}, \tag{2.10}$$

where $\Xi^{\alpha}_{JI}(\tau) = \dot{\boldsymbol{R}}^{\alpha}\cdot \boldsymbol{d}^{\alpha}_{JI}(\tau)$, and a hop occurs if and only if

$$\sum_{K\leqslant J-1} g^{\alpha}_{IK} < \zeta < \sum_{K\leqslant J} g^{\alpha}_{IK}, \tag{2.11}$$

where ζ is generated randomly in the interval $[0,1]$. In practice, a swarm of trajectories is propagated independently starting from different initial conditions, and the final statistical distribution of all these trajectories is assumed to reproduce the final density probability given by the nuclear wave packet.

B. Interaction Hamiltonian to LCT

Upon interaction with a radiation field, the full Hamiltonian becomes

$$\hat{H} = \hat{H}_0 + \hat{H}_{\mathrm{int}}, \tag{2.12}$$

where $\hat{H}_0$ is the field-free Hamiltonian and $\hat{H}_{\mathrm{int}}$ is the interaction Hamiltonian expressed with the Coulomb gauge,

$$\hat{H}_{\mathrm{int}} = -\frac{e}{2m_e c}\sum_i \boldsymbol{A}(\boldsymbol{r}_i,t)\cdot\hat{\boldsymbol{p}}_i, \tag{2.13}$$

where $\boldsymbol{A}(\boldsymbol{r},t)$ is the (classical) vector potential of the electromagnetic field, $\hat{\boldsymbol{p}}_i$ is the momentum operator of electron i, e is the electron charge, m_e is the electron mass, and c is the speed of light. By using the dipole approximation, this can be expressed as

$$\langle \hat{H}_{\mathrm{int}}\rangle_{JI} = i\omega_{JI}\frac{\boldsymbol{A}_0}{c}\cdot\boldsymbol{\mu}_{JI}e^{-i\omega t}, \tag{2.14}$$

which, through the relation $\boldsymbol{E}(t) = -\frac{1}{c}\frac{\partial}{\partial t}\boldsymbol{A}(t)$, can be written in the more common form as

$$\langle \hat{H}_{\mathrm{int}}\rangle_{JI} = -\boldsymbol{\mu}_{JI}\cdot\boldsymbol{E}_0 e^{-i\omega t} = -\boldsymbol{\mu}_{JI}\cdot\boldsymbol{E}(t). \tag{2.15}$$

In the presence of an external radiation field, the equation of motions in Eq. (2.9) becomes

$$i\hbar\dot{C}^{\alpha}_{J}(t) = \sum_I C^{\alpha}_I(t)\left[H_{JI} - i\hbar\dot{\boldsymbol{R}}^{\alpha}\cdot\boldsymbol{d}^{\alpha}_{JI} - \boldsymbol{\mu}^{\alpha}_{JI}\cdot\boldsymbol{E}(t)\right], \tag{2.16}$$

where $\boldsymbol{\mu}^{\alpha}_{JI}$ is the position dipole vector between states I and J. Minor adaptations to Tully's hopping scheme are described in Ref. [19].

The aim of LCT is to calculate an electric field on-the-fly as a function of the dynamics at each time step to ensure the increase (or decrease) in some predefined expectation value. If we consider the time evolution of an arbitrary operator $\mathcal{O}$, one finds

$$\dot{\mathcal{O}}(t) = \frac{i}{\hbar}\int \Psi^*(\boldsymbol{r},\boldsymbol{R},t)[\hat{H}_0,\mathcal{O}]\Psi(\boldsymbol{r},\boldsymbol{R},t)d\boldsymbol{r}\,d\boldsymbol{R} + \int \Psi^*(\boldsymbol{r},\boldsymbol{R},t)[\hat{H}_{\mathrm{int}},\mathcal{O}]\Psi(\boldsymbol{r},\boldsymbol{R},t)d\boldsymbol{r}\,d\boldsymbol{R}. \tag{2.17}$$

This equation shows that, if $\mathcal{O}$ and $\hat{H}_{\mathrm{int}}$ do not commute, it is possible to influence the changes in the expectation of $\mathcal{O}$ with a shaped external field. Assuming that $\hat{H}_0$ commutes with $\mathcal{O}$, which is only true in the absence of NACs, Eq. (2.17) can be written as

$$\dot{\mathcal{O}}(t) = -\boldsymbol{E}(t)\frac{i}{\hbar}\int \Psi^*(\boldsymbol{r},\boldsymbol{R},t)[\hat{\mu},\mathcal{O}]\Psi(\boldsymbol{r},\boldsymbol{R},t)d\boldsymbol{r}\,d\boldsymbol{R}, \tag{2.18}$$

and therefore, the control is achieved by changing the temporal evolution of $\boldsymbol{E}$. We note that, in the presence of NACs, Eq. (2.18) will contain an additional time-dependent term. To control the population transfer for a particular electronic state $|I\rangle$, the projector operator $\mathcal{P}_I = |I\rangle\langle I|$ is used. The time evolution of the state population can then be written as

$$\dot{\mathcal{P}}_I(t) = -\boldsymbol{E}(t)\frac{i}{\hbar}\int \Psi^*(\boldsymbol{r},\boldsymbol{R},t)[\hat{\mu},\mathcal{P}_I]\Psi(\boldsymbol{r},\boldsymbol{R},t)d\boldsymbol{r}\,d\boldsymbol{R}. \tag{2.19}$$

By expanding the projector and using the ansatz (2.8) for a trajectory α, this becomes

$$\dot{\mathcal{P}}^{\alpha}_I(t) = -2\boldsymbol{E}^{\alpha}(t)\sum_J \mathrm{Im}\left[C^{\alpha *}_J(t)\boldsymbol{\mu}_{JI}C^{\alpha}_I(t)\right]. \tag{2.20}$$

From this equation, it is clear that choosing the electric field to be

$$\boldsymbol{E}^{\alpha}(t) = \pm\lambda\sum_J \mathrm{Im}\left[C^{\alpha *}_J(t)C^{\alpha}_I(t)\boldsymbol{\mu}_{JI}\right] \tag{2.21}$$

ensures that $\dot{\mathcal{O}}(t)$ increases (or decreases) at all times.

III. METHODS AND COMPUTATIONAL DETAILS

The focus of our paper is the alkali halide molecule LiF. The ground state (GS) of LiF, $1^1\Sigma^+$, is followed by a doubly degenerate $1^1\Pi^+$ state (here referred to as the first excited state) and a $2^1\Sigma^+$ state (second excited state); these are represented in the potential-energy curves shown in Fig. 1. The equilibrium bond distance is 1.59 Å within DFT-Perdew-Burke-Ernzerhof (PBE) and a plane-wave basis set (experimental value: 1.5639 Å, CAM-B3LYP/aug-cc-pVDZ: 1.58 Å). At larger distances from equilibrium, the GS and first excited state correlate with the $^2S(\mathrm{Li}) + {}^2P(\mathrm{F})$ dissociation channel, and the second excited state correlates with the still bound $^1S(\mathrm{Li}^+) + {}^1S(\mathrm{F}^-)$ channel. More details can be found in Refs. [19,40] and Supplemental Material [41].

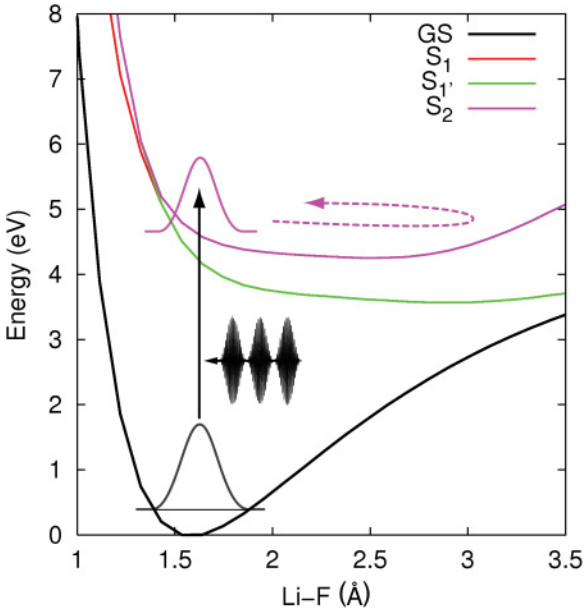

FIG. 1. (Color online) Potential-energy curve of the GS and first two excited states of the LiF molecule. Energies (LR-TDDFT–PBE-TDA) are given with respect to the GS (DFT-PBE).

The nonadiabatic MD was implemented within the CPMD package [35], and the system was composed of an isolated LiF molecule, aligned along the x axis of a box of dimensions 14 Å × 8 Å × 8 Å. All calculations employed Goedecker-type pseudopotentials [42–44], a cutoff of 120 Ry for the plane-wave basis set, and a threshold of 10^{-7} a.u. for the convergence of the orbitals. The GS (S_0) and first two excited states (S_1 and S_2) were included in the simulation, and the LR-TDDFT equations were solved within the Tamm-Dancoff approximation (TDA) to obtain the unperturbed excitation energies and nuclear forces [45]. The adiabatic approximation was used for the xc kernel, and the xc-functional PBE [46] was employed. The initial geometries were sampled from a canonical distribution at 100 K obtained from GS Born-Oppenheimer MD. From this equilibrated GS distribution, different initial configurations were randomly selected and were considered as starting points for the nonadiabatic dynamics. Initial velocities were set equal to the corresponding GS values.

The exact propagation of the nuclear wave packet was performed using the Heidelberg MCTDH package [47]. The potential-energy curves and transition dipole were taken from DFT-PBE and LR-TDDFT–PBE-TDA calculations, with the potential being quadratically interpolated within the code between points every 0.1 Å. Only the two electronic states of interest (S_0 and S_2) were included because the NACs between S_2 and S_1, as mentioned above, were found to be negligible. The propagation was performed on a fast Fourier transform (FT) grid with 551 points between 0.8 and 3.5 Å. The initial wave packet was centered at 1.59 Å with 0.2-Å width.

The objective was to control the population transfer from the GS to S_2 (Fig. 1). Within the LCT algorithm, there are three parameters, λ, the strength factor shown in Eq. (2.21), the seed strength, and seed time. A seed was required because initially the population of S_2 was zero, and as shown in Eq. (2.21), in this scenario, the pulse and, therefore, the population will remain zero at all times. In both cases, the seed strength was 0.004 a.u., and the seed time was 2.5 fs. In the QD simulations, $\lambda = 0.0622$, and for the TSH simulations, $\lambda = 0.3185$; the reason for the difference is discussed in Sec. V.

IV. RESULTS

In this section, we present the results in the following manner; first, a TSH calculation with a pulse containing only the resonance frequency of the S_0–S_2 transition is shown, and then, in Sec. IV B, we use LCT in conjunction with QD. These results form a reference that allows us, in the final section, to provide a detailed analysis of the results obtained from the implementation of LCT using the TSH framework within the CPMD package.

We will make use of the following definitions: the square of the amplitude for a specific trajectory $|C_J(t)|^2$ will be called probability to be on state J, whereas, $P_J(t)$ will denote its actual population, which is either 0 or 1 for a single trajectory. The average over a swarm of trajectories leads to the corresponding average values for the probabilities $\langle |C_J(t)|^2 \rangle_n$ and the populations $\langle P_J(t) \rangle_n$, where n is the total number of trajectories (Fig. 6).

A. Resonant frequency pulse with trajectories

First, as a reference, we consider the effect of a pulse containing a single resonant frequency. In Fig. 2, we show the temporal evolution of the population in each state during perturbation by an external field with frequency $\omega = 0.17$ a.u. and functional form expressed as $\boldsymbol{A}(t) = -A_0 \boldsymbol{\epsilon}^{\lambda} \exp(-\frac{(t-t_0)^2}{T^2}) \sin(\omega t)$. t_0 and T are set equal to 100 and 67 fs, respectively, which produces a pulse of a duration of ∼200 fs with a polarization vector $\boldsymbol{\epsilon}^{\lambda} = (1,0,0)$. More details can be found in Refs. [19,40].

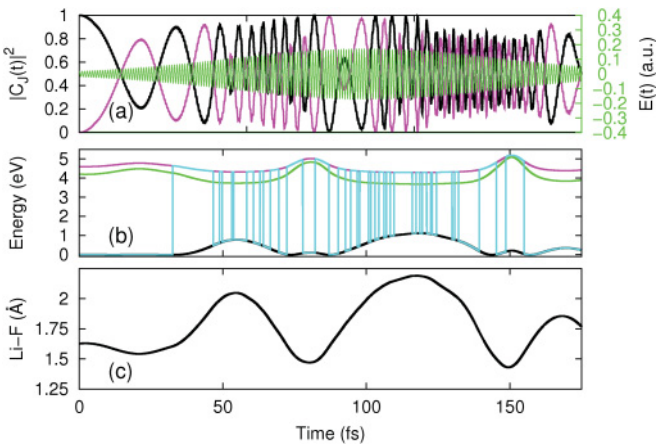

FIG. 2. (Color online) LiF under a polarized pulse, $\omega = 0.17$ a.u. and $A_0/c = 1.0$ a.u. (a) Probability ($|C_J(t)|^2$) of each state for one trajectory. Color code: black, GS and blue (dark gray), second excited state (S_2). Green (medium gray) line and left axis show the electric field used. (b) Potential-energy curves during the dynamics obtained by DFT-PBE and LR-TDDFT–PBE-TDA calculations. Pale blue (light gray) line highlights the running state. (c) Bond length of LiF during the simulation.

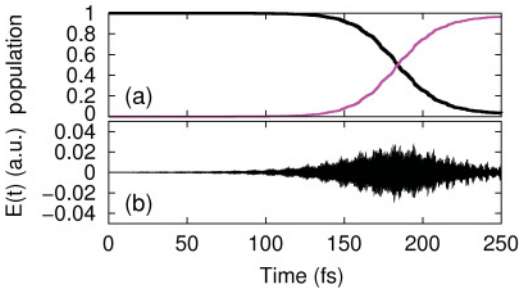

FIG. 3. (Color online) Local control from QD. (a) Population transfer from S_0, black line, to S_2, red (gray) line. (b) Calculated pulse (λ value of 0.0622 a.u.).

The effect of this field causes amplitude transfer analogous to Rabi oscillations, and although there is a significant probability on the S_2 state (large $|C_2(t)|^2$), this is never populated in a stable way. This also is reflected by the dynamics of the running state [electronic state from which nuclear forces are computed, Fig. 2(c)], which shows how the trajectory does not remain on S_2 but instead, constantly *hops* between S_0 and S_2.

B. Local control with QD

In Fig. 3, we present the population transfer between the states S_0 and S_2 and the corresponding pulse for the QD simulation, which makes use of the potential-energy curves and transition dipole extracted from DFT-PBE and LR-TDDFT–PBE-TDA calculations. This result shows a transfer of population close to 100%, within 250 fs. The pulse has a maximum intensity of 0.025 a.u., well within the weak-field limit.

The temporal profile of the pulse clearly shows the superposition of a number of frequencies which are resolved using a FT (Fig. 7, upper panel). The most prominent of these, at 4.25 eV, corresponds, unsurprisingly, to the energy gap between the two states when the bond length is around 2 Å, the point at which population transfer occurs. The second largest peak in the FT is at 3.25 eV, exactly 1.0 eV lower and corresponds to the oscillations of the wave packet in the GS [Fig. 9(a), upper panel], which has a time period of around 4 fs. We also observe two frequencies, shifted 0.3 eV from the peaks at 3.25 and 4.25 eV. These correspond to the oscillations of the wave packet in the excited state [Fig. 9(b)].

C. Local control with trajectories

Figures 4 and 5 show the time evolution of the probabilities ($|C_J(t)|^2$), calculated pulse, and potential-energy curves for two different trajectories computed using LCT within TSH (three other trajectories are reported in the Supplemental Material [48]). In each case, we observe, at least, a 95% transfer of probability to S_2 within 200 fs, and the trajectory hops onto the target state between 150 and 175 fs, typically, when the probabilities of the two states are equivalent. These results show a marked difference to that obtained using a single resonant frequency pulse in Fig. 2. On the other hand, the agreement with the QD simulations on the amplitude transfer and timescales is generally very good.

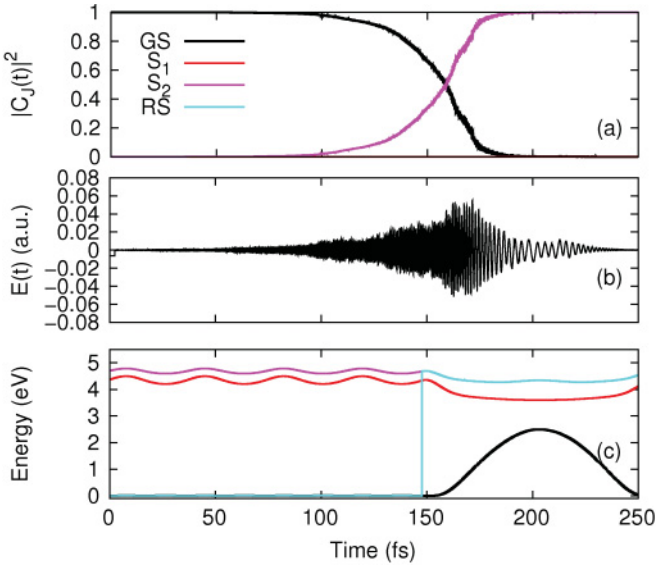

FIG. 4. (Color online) LCT within TSH, trajectory 1. (a) Probabilities of each state. General color code: black, GS; red (gray), doubly degenerate $1^1\Pi^+$ first excited state; green (medium gray), second excited state $2^1\Sigma^+$ (S_2). (b) Calculated LCT pulse (c) Potential-energy curves along the dynamics obtained by DFT-PBE and LR-TDDFT–PBE-TDA calculations. Pale blue (light gray) line highlights the running state.

In a process driven by the product of the amplitudes on each state [see Eq. (2.21)], the population transfer is initially slow due to the small amount of amplitude on S_2 at time $t = 0$. In fact, in all cases, little or no transfer occurs within the first 100 fs in agreement with the QD calculations. In Fig. 4(c), we plot the running state on top of the potential-energy curves (see also Supplemental Material [48] for additional trajectories). This shows that, once the trajectory has jumped to S_2, it remains in the excited state for the rest of the simulation.

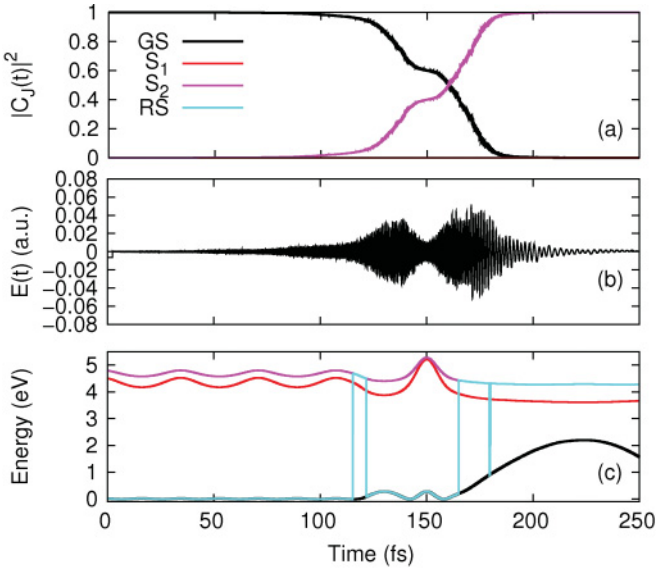

FIG. 5. (Color online) LCT within TSH, trajectory 2. For the description of panels (a)–(c) and the color coding, see caption of Fig. 4.

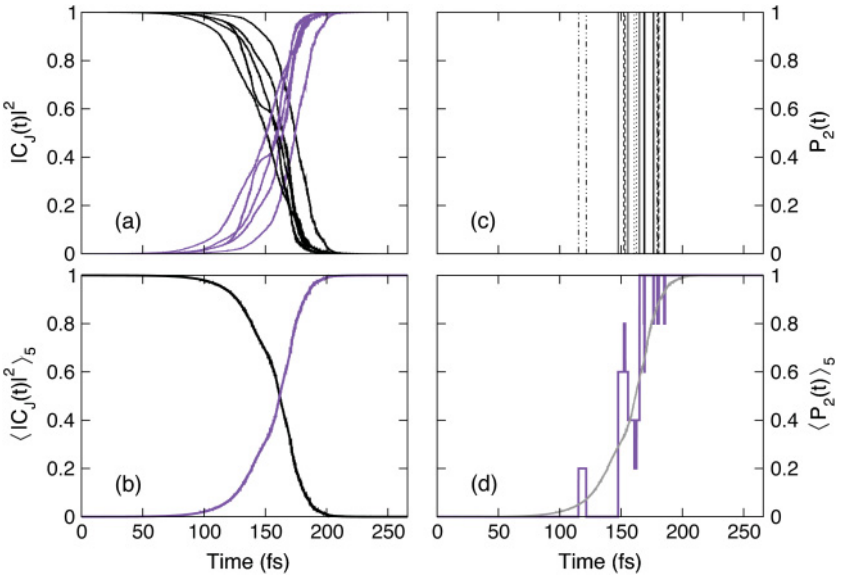

FIG. 6. (Color online) Time evolution of (a) the probabilities $|C_J(t)|^2$ for five trajectories (S_0 in black and S_2 in magenta), (b) the average of the probabilities $\langle |C_J(t)|^2 \rangle_5$ over five trajectories, (c) the population of state S_2 $P_2(t)$ for each trajectory (a different line style represents a different trajectory), and (d) the average population of state S_2 over five trajectories $\langle P_2(t) \rangle_5$ (light gray line represents $\langle |C_J(t)|^2 \rangle_5$).

This contrasts with results obtained for the unoptimized pulse (Fig. 2) where the trajectory frequently *hops* between the two states. It is interesting to note that the statistics collected over five trajectories for the population of state S_2 ($\langle P_2(t) \rangle_5$) and the different probabilities ($\langle |C_J(t)|^2 \rangle_5$) are in close agreement with each other (see Fig. 6). However, we note that many more trajectories would be needed to fully converge the TSH calculation and, therefore, to obtain a smoother time evolution in Figs. 6(c) and 6(d).

The agreement between TSH and QD calculations also extends to the shape of the calculated pulses [Fig. 4(b) and Supplemental Material [48]. In part, this is probably due to the simplicity of the system under study, however, it also reflects the simple nature of the control strategy. An exception is reported in Fig. 5, where we show a case in which the TSH dynamics produces a pulse with a double envelope. This is due to a back jump from S_2 to S_0 at $\sim$125 fs, which leads to a compression of the LiF bond [see Fig. 5(c) at $t = 150$ fs]. At this geometry, the transition dipole to S_2 becomes much smaller due to the mixing with other electronic states, and, as a consequence, a stop in the growth (decline) of the population of S_2 (GS) is observed. This is also reflected in the overall shape of the pulse in the same time interval [Fig. 5(b)].

The FT of the calculated pulses (Fig. 7) shows that the largest frequency contribution occurs at 4.75 eV, which corresponds to the energy gap between the two electronic states considered. This value is slightly shifted (0.5 eV) compared to the one obtained in the QD simulation (4.25 eV) and is a result of the classical nature of the TSH dynamics. Finally, the second timescale of about 40 fs corresponds to the period of the oscillation of the trajectory in the GS (Fig. 9).

V. DISCUSSION

In the following section, we discuss some important observations of the paper, and we pay particular attention to the comparison between TSH and the nuclear QD.

In TSH, unlike QD where the nuclear wave packet on the excited state will evolve under the forces of that state, one can have amplitude on S_2 even though the forces on the nuclei are derived from S_0 (see pictorial representation in Fig. 8). In fact, contrary to QD, amplitude in TSH does not affect the nuclear dynamics directly because change in the driving forces only occurs after a surface hop (population transfer).

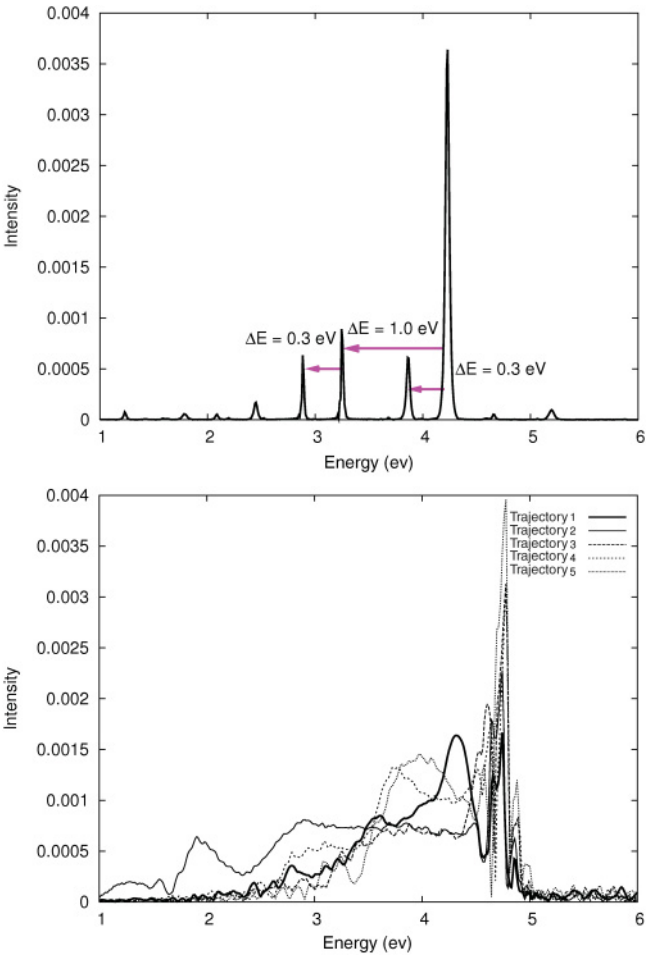

FIG. 7. (Color online) (Upper panel) FT of the control pulse in QD. (Lower panel) FT of the control-pulse calculations for five trajectories (a different line style represents a different trajectory).

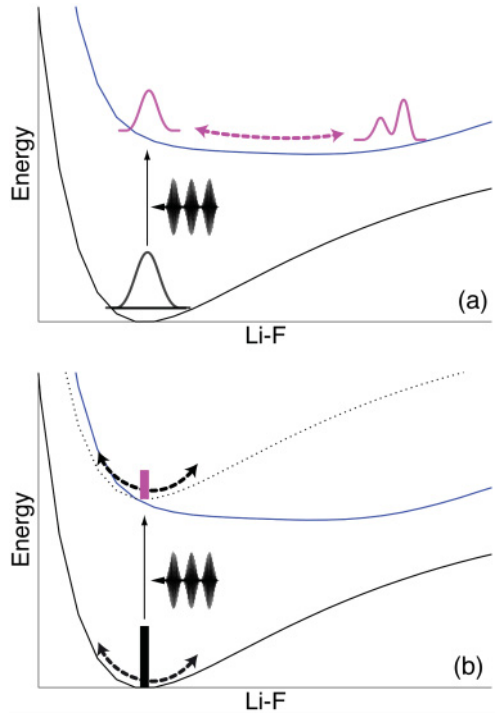

FIG. 8. (Color online) Pictorial representation of the differences between (a) wave packet and (b) independent trajectory propagation schemes. For a wave-packet, propagation population transferred on the excited state will evolve as a function of the forces of that state. However, in independent trajectory-based approaches, amplitude on the excited state evolves on the running state of the trajectory.

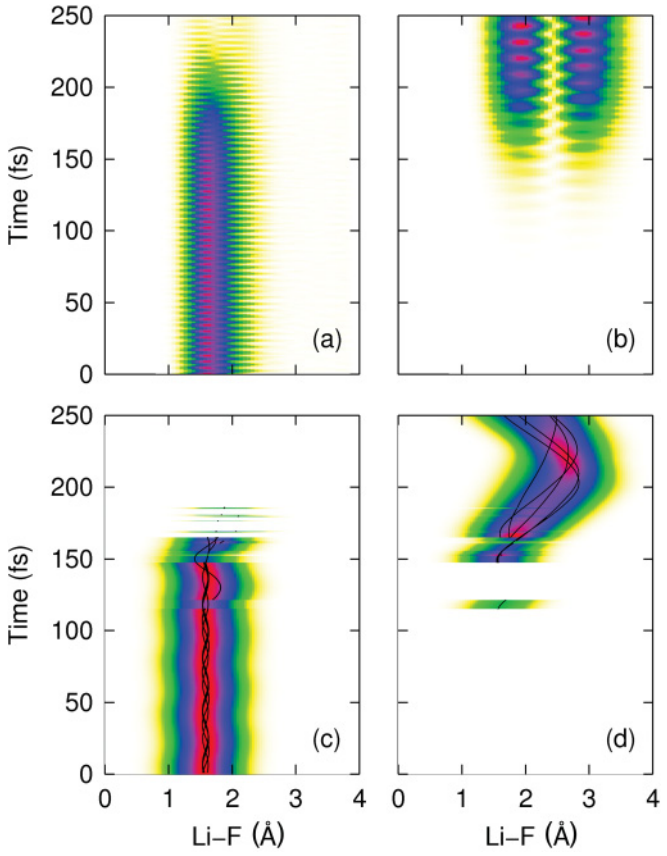

FIG. 9. (Color online) (Upper panel) Time evolution of the probability density of the nuclear wave packet on (a) S_0 and (b) S_2 during the control propagation of Fig. 3. (Lower panel) Time evolution of the LiF bond length for each TSH trajectory during the control. Each trajectory (black line) has been artificially broadened by a Gaussian with a full width at half maximum of 0.68 Å, and the resulting sum over all frozen Gaussians is represented. (c) Trajectories are running on S_0 and (d) on S_2 during the control propagation. The unit of the intensity is arbitrary.

Furthermore, simultaneous population of both states does not occur in TSH because of the ITA that cancels correlation between trajectories. The correct population of the different states as a function of time cannot be obtained on-the-fly when trajectories are computed sequentially, but it is recovered *a posteriori* from the statistics collected over subsequent runs [see Figs. 6(c) and 6(d)]. As a consequence, superposition effects between GS and excited-state dynamics observed in QD are absent in TSH. These differences are reflected in the shape of the computed pulses, which we will now discuss.

In QD, both the GS and the excited-state frequencies contribute to the pulse over the entire length of the excitation dynamics because of the superposition between the GS and the excited-state wave functions. On the contrary, in TSH, the produced pulse oscillates at the frequency of the GS until a surface hop to the excited state occurs. Once the trajectory reaches the excited state, we observe a sudden decrease in the frequency to the value characteristic for the excited state, which produces a chirping of the pulse (see Fig. 4). The same argument can also be used to explain the difference in the magnitude of the coupling constant λ [Eq. (2.21)] used in the two approaches to achieve excitation over the same time period. In QD, the progressive population of S_2 induces a continuous increase in the bond length with consequent growth of the transition dipole $\boldsymbol{\mu}_{IJ}$, which favors the excitation. On the contrary, in TSH, even though amplitude is transferred from the very beginning of the pulse, elongations of the bond (and corresponding increase in the coupling with the external field) only occur after a surface hop [Figs. 9(c) and 9(d)], causing a delay in the excitation.

In Sec. IV, we noted that the calculated pulse from TSH possessed a weak periodic oscillation with a period of 40 fs, which is not present in the pulse calculated using QD. This corresponds to the oscillatory period of the classical trajectory in the GS [Fig. 9(c)] and reflects the increased coupling strength (high transition dipole moment) at the classical turning points on S_0. Instead, in QD, since the expectation value of the bond length does not change, the wave packet remains mainly stationary at its equilibrium position [Fig. 9(a)], resulting in no change in the transition dipole moment at the classical bond-length frequency.

Another interesting observation comes from the comparison of the exact nuclear wave-packet dynamics (from QD) with the reconstructed classical wave packet obtained from the collection of the TSH trajectories [five trajectories, each broadened by a frozen Gaussian with a full width at half maximum of 0.68 Å, the sum of the different contributions is represented in Figs. 9(c) and 9(d)]. In fact, even though each trajectory represents the time evolution of classical nuclei, the time

evolution of the ensemble of trajectories in TSH can reproduce, at least approximately, the nuclear wave-packet dynamics [49]. In the first part of the trajectory (first 150 fs in the GS), both methods describe a stationary system characterized by a LiF bond-length distribution centered at the S_0 average value ($\sim$1.5 Å, see Fig. 9). When excitation to S_2 occurs, QD shows the typical pattern of a vibrational excitation $v = 1$, whereas, the trajectory-based method exhibits large amplitude oscillations of the LiF bond length. After broadening of the trajectories, the reconstructed TSH wave packet presents maximum probability density at the turning points of the trajectories, as expected in the case of classical trajectories. This example clearly shows how the collection of a swarm of trajectories obtained with Tully's TSH, using classical trajectories, can only describe the correct QD of the system approximately, while pure quantum effects, such as the quantization of vibrational modes, quantum coherence, and tunneling cannot be captured by this approach. It is important to mention that a larger number of trajectories is required in order to fully converge the TSH calculation and, therefore, to obtain a smoother time evolution in Figs. 9(c) and 9(d).

VI. CONCLUSION

In this paper, we combined LCT with the recently developed on-the-fly LR-TDDFT-based nonadiabatic TSH dynamics [14] and compared its predictions with those obtained from the exact wave-packet dynamics. LCT uses the instantaneous dynamics of the system to calculate the pulse shape that ensures the desired change in the expectation value of a given operator. This approach does not require the optimization of any target functionals as in OCT in which gradients are computed using Lagrangian multiplier techniques based on the computationally expensive forward and backward propagations of the equations of motion. In this sense, LCT provides a valid alternative formulation of the problem, even though the optimization of the laser pulse present in the OCT formulation may be important for complex control of a global wave function. We note, at this point, that there are connections between LCT and OCT; in some cases, using Krotov's scheme yields the LCT equation [34].

We applied LCT to the study of the photodynamics of a simple linear molecule, LiF. In this case, the target quantity is simply the population amplitude of the bound excited state S_2. Our approach is able to efficiently compute an electric field able to achieve almost complete amplitude transfer from the GS to S_2 within approximately 250 fs. This represents a significant improvement compared to the effect of a simple monochromatic electric field at the resonant energy. The agreement between the QD and TSH results is surprisingly good for both the length and shape of the pulse and the underlying dynamics. The differences observed, for instance, in the shift of the main pulse frequency and in the excited-state dynamics, are mainly due to the classical nature of an individual TSH trajectory and, in particular, to the enforced locality introduced by the ITA. We, therefore, expect better agreement with the QD results when correlated trajectory-based approaches [49–53] are used in place of Tully-type TSH.

Finally, we would like to point out that the pulses calculated in this paper are well within the weak-field limit with a temporal resolution of $\sim$150 fs. Such pulses are within the capabilities of modern laser sources, and therefore, an experiment to confirm these findings could be performed. However, more interesting would be to extend this approach to larger systems within a quantum mechanical-molecular mechanical framework including the dissipative effects of the environment. Even though such an extension would pose a much greater experimental and theoretical challenge, the analysis of the shaped pulse eventually can give important insight into the dynamics of the system, identifying characteristic times of the vibrational modes involved in the specific targeted excitation. This becomes especially important when complex systems with a large number of degrees of freedom are studied.

The combination of LCT with an efficient method for the computation of nonadiabatic dynamics offers different opportunities in the discovery of chemical routes that include activation steps triggered by properly shaped pulses.

ACKNOWLEDGMENTS

The authors thank the CADMOS project for the computer time. COST Action CM0702, Swiss NSF Grant No. 200020-130082, and the NCCR-MUST interdisciplinary research program are acknowledged for funding.

[1] J. C. Tully, J. Chem. Phys. **93**, 1061 (1990).
[2] E. Tapavicza, I. Tavernelli, U. Rothlisberger, C. Filippi, and M. E. Casida, J. Chem. Phys. **129**, 124108 (2008).
[3] R. Mitrić, V. Bonačić-Koutecký, J. Pittner, and H. Lischka, J. Chem. Phys. **125**, 24303 (2006).
[4] M. Barbatti and H. Lischka, J. Phys. Chem. A **111**, 2852 (2007).
[5] M. Vazdar, M. Eckert-Maksić, M. Barbatti, and H. Lischka, Mol. Phys. **107**, 845 (2009).
[6] M. Barbatti, G. Granucci, M. Persico, M. Ruckenbauer, M. Vazdar, M. Eckert-Maksic, and H. Lischka, J. Photochem. Photobiol. A **190**, 228 (2007).
[7] U. Werner, R. Mitrić, T. Suzuki, and V. Bonačić-Koutecký, Chem. Phys. **349**, 319 (2008).
[8] M. Barbatti, WIRES: Comput. Molec. Sci. **1**, 620 (2011).
[9] E. Runge and E. K. U. Gross, Phys. Rev. Lett. **52**, 997 (1984).
[10] E. K. U. Gross and W. Kohn, Phys. Rev. Lett. **55**, 2850 (1985).
[11] M. E. Casida, in *Recent Advances in Density Functional Methods*, edited by D. P. Chong (Singapore, World Scientific, 1995), p. 155.
[12] M. Petersilka, U. J. Gossmann, and E. K. U. Gross, Phys. Rev. Lett. **76**, 1212 (1996).
[13] H. Appel, E. K. U. Gross, and K. Burke, Phys. Rev. Lett. **90**, 043005 (2003).

[14] E. Tapavicza, I. Tavernelli, and U. Rothlisberger, Phys. Rev. Lett. **98**, 023001 (2007).
[15] I. Tavernelli, E. Tapavicza, and U. Rothlisberger, J. Chem. Phys. **130**, 124107 (2009).
[16] I. Tavernelli, E. Tapavicza, and U. Rothlisberger, J. Mol. Struct., Theochem **914**, 22 (2009).
[17] I. Tavernelli, B. F. E. Curchod, and U. Rothlisberger, J. Chem. Phys. **131**, 196101 (2009).
[18] I. Tavernelli, B. F. E. Curchod, A. Laktionov, and U. Rothlisberger, J. Chem. Phys. **133**, 194104 (2010).
[19] I. Tavernelli, B. F. E. Curchod, and U. Rothlisberger, Phys. Rev. A **81**, 052508 (2010).
[20] R. Mitrić, J. Petersen, and V. Bonačić-Koutecký, Phys. Rev. A **79**, 053416 (2009).
[21] J. Petersen, R. Mitrić, V. Bonačić-Koutecký, J.-P. Wolf, J. Roslund, and H. Rabitz, Phys. Rev. Lett. **105**, 073003 (2010).
[22] R. Mitrić, J. Petersen, M. Wohlgemuth, U. Werner, V. Bonačić-Koutecký, L. Woeste, and J. Jortner, J. Phys. Chem. A **115**, 3755 (2011).
[23] R. Mitrić, J. Petersen, M. Wohlgemuth, U. Werner, and V. Bonačić-Koutecký, Phys. Chem. Chem. Phys. **13**, 8690 (2011).
[24] M. Richter, P. Marquetand, J. González-Vázquez, I. Sola, and L. González, J. Chem. Theory Comput. **7**, 1253 (2011).
[25] D. J. Tannor and S. A. Rice, J. Chem. Phys. **83**, 5013 (1985).
[26] P. Brumer and M. Shapiro, Chem. Phys. Lett. **126**, 541 (1986).
[27] A. P. Peirce, M. A. Dahleh, and H. Rabitz, Phys. Rev. A **37**, 4950 (1988).
[28] R. S. Judson and H. Rabitz, Phys. Rev. Lett. **68**, 1500 (1992).
[29] P. Marquetand, C. Meier, and V. Engel, J. Chem. Phys. **123**, 204320 (2005).
[30] S. Graefe and V. Engel, Chem. Phys. **329**, 118 (2006).
[31] P. Marquetand and V. Engel, J. Chem. Phys. **127**, 084115 (2007).
[32] T. J. Penfold, G. A. Worth, and C. Meier, Phys. Chem. Chem. Phys. **12**, 15616 (2010).
[33] R. Kritzer, C. Meier, and V. Engel, Chem. Phys. Lett. **477**, 75 (2009).
[34] V. Engel, C. Meier, and D. J. Tannor, Adv. Chem. Phys. **141**, 29 (2009).
[35] CPMD (Copyright IBM Corp 1990–2001, Copyright MPI für Festkörperforschung Stuttgart, 1997–2001), [http://www.cpmd.org].
[36] M. H. Beck, A. Jäckle, G. A. Worth, and H. D. Meyer, Phys. Rep. **324**, 1 (2000).
[37] G. A. Worth, P. Hunt, and M. A. Robb, J. Phys. Chem. A **107**, 621 (2003).
[38] T. J. Penfold and G. A. Worth, J. Mol. Graphics Modell. **26**, 613 (2007).
[39] M. Born and K. Huang, *Dynamical Theory of Crystal Lattices* (Clarendon, Oxford, 1954).
[40] K. Yagi and K. Takatsuka, J. Chem. Phys. **123**, 224103 (2005).
[41] See Supplemental Material at http://link.aps.org/supplemental/10.1103/PhysRevA.84.042507, for an orbital picture of the electronic states.
[42] S. Goedecker, M. Teter, and J. Hutter, Phys. Rev. B **54**, 1703 (1996).
[43] C. Hartwigsen, S. Goedecker, and J. Hutter, Phys. Rev. B **58**, 3641 (1998).
[44] M. Krack, Theor. Chem. Acc. **114**, 145 (2005).
[45] J. Hutter, J. Chem. Phys. **118**, 3928 (2003).
[46] J. P. Perdew, K. Burke, and M. Ernzerhof, Phys. Rev. Lett. **77**, 3865 (1996).
[47] G. A. Worth, M. H. Beck, A. Jäckle, and H.-D. Meyer, *The Heidelberg MCTDH Package: A Set of Programs for Multidimensional Quantum Dynamics* (Heidelberg University Press, Heidelberg, 2000), User's Guide, Version 8 (the User's Guide can be downloaded from the URL: http://www. pci.uni-heidelberg.de/tc/usr/mctdh/).
[48] See Supplemental Material at http://link.aps.org/supplemental/10.1103/PhysRevA.84.042507, for the time evolution of the probabilities, calculated pulse, and potential-energy curves for three additional trajectories using LCT.
[49] B. F. E. Curchod, I. Tavernelli, and U. Rothlisberger, Phys. Chem. Chem. Phys. **13**, 3231 (2011).
[50] R. E. Wyatt, C. L. Lopreore, and G. Parlant, J. Chem. Phys. **114**, 5113 (2001).
[51] C. L. Lopreore and R. E. Wyatt, J. Chem. Phys. **116**, 1228 (2002).
[52] S. Garashchuk, V. A. Rassolov, and G. C. Schatz, J. Chem. Phys. **123**, 174108 (2005).
[53] B. Poirier and G. Parlant, J. Phys. Chem. A **111**, 10400 (2007).